Geochemistry, Geophysics, Geosystems®

AGU ADVANCING EARTH AND SPACE SCIENCE

RESEARCH ARTICLE
10.1029/2022GC010350

The Sediment Green-Blue Color Ratio as a Proxy for Biogenic Silica Productivity Along the Chilean Margin

Chen Li[1,2], Vincent J. Clementi[1], Samantha C. Bova[1,3], Yair Rosenthal[1,4], Laurel B. Childress[5], James D. Wright[4], Zhimin Jian[2], and Expedition 379T Scientists[6]

[1]Department of Marine and Coastal Sciences, Rutgers University, New Brunswick, NJ, USA, [2]State Key Laboratory of Marine Geology, Tongji University, Shanghai, China, [3]Now at Department of Geological Sciences, San Diego State University, San Diego, CA, USA, [4]Department of Earth and Planetary Sciences, Rutgers University, New Brunswick, NJ, USA, [5]International Ocean Discovery Program, Texas A&M University, College Station, TX, USA, [6]See Appendix A

Abstract Sediment cores recently collected from the Chilean Margin during D/V *JOIDES Resolution* Expedition 379T (JR100) document variability in shipboard-generated records of the green/blue (G/B) ratio. These changes show a strong coherence with benthic foraminiferal $\delta^{18}O$, Antarctic ice core records, and sediment lithology (e.g., higher diatom abundances in greener sediment intervals), suggesting a climate-related control on the G/B. Here, we test the utility of G/B as a proxy for diatom productivity at Sites J1002 and J1007 by calibrating G/B to measured biogenic opal. Strong exponential correlations between measured opal% and the G/B were found at both sites. We use the empirical regressions to generate high-resolution records of opal contents (opal%) on the Chilean Margin. Higher productivity tends to result in more reducing sedimentary conditions. Redox-sensitive sedimentary U/Th generally co-varies with the reconstructed opal% at both sites, supporting the association between sediment color, sedimentary U/Th, and productivity. Lastly, we calculated opal mass accumulation rate (MAR) at Site J1007 over the last ~150,000 years. The G/B-derived opal MAR record from Site J1007 largely tracks existing records derived from traditional wet-alkaline digestion from the south and eastern equatorial Pacific (EEP) Ocean, with a common opal flux peak at ~50 ka suggesting that increased diatom productivity in the EEP was likely driven by enhanced nutrient supply from the Southern Ocean rather than dust inputs as previously suggested. Collectively, our results identify the G/B ratio as a useful tool with the potential to generate reliable, high-resolution paleoceanographic records that circumvent the traditionally laborious methodology.

Plain Language Summary The color of marine sediments often corresponds to oceanic and sedimentary processes that can influence the global climate system. Visual inspection of new sediment cores collected from the Chilean Margin revealed substantial downcore changes in green and blue sediment colors. Greener sediment intervals were usually enriched with diatoms, whereas bluer sediments were rich in clay minerals. A specialized camera was used to scan the cores and enable us to quantitatively describe the core colors using the green/blue (G/B) ratio. The similarity of the downcore G/B ratio with Antarctic ice core records suggests that it may serve as a quick tool to estimate the age of the cores during the cruise. In this paper, we show that changes in the G/B ratio are a function of diatom (biogenic opal) productivity and use a calibrated relationship to calculate a continuous record of opal flux at the Chilean Margin over the last 150,000 years. A distinct opal flux maxima at 50,000 years ago is observed, similar to previous studies in the eastern equatorial Pacific. This common event implies a tight link between the high- and low-latitude eastern Pacific Ocean, potentially attributable to enhanced nutrient supply from the Southern Ocean.

Chen Li and Vincent J. Clementi contributed equally to this work.

Key Points:

- Sediment green-to-blue ratio serves as a novel proxy for changes in diatom productivity on the Chilean Margin
- High-resolution opal mass accumulation rates derived from green-to-blue ratio agree with existing records for the last 150 kyr
- The green-to-blue ratio proxy is potentially applicable in other regions of high diatom productivity with a site-specific calibration

Supporting Information:

Supporting Information may be found in the online version of this article.

Correspondence to:

C. Li and V. J. Clementi,
1532983@tongji.edu.cn;
clementi@marine.rutgers.edu

Citation:

Li, C., Clementi, V. J., Bova, S. C., Rosenthal, Y., Childress, L. B., Wright, J. D., et al. (2022). The sediment green-blue color ratio as a proxy for biogenic silica productivity along the Chilean Margin. *Geochemistry, Geophysics, Geosystems*, *23*, e2022GC010350. https://doi.org/10.1029/2022GC010350

Received 18 JAN 2022
Accepted 25 APR 2022

1. Introduction

Variations in Southern Ocean and South Pacific primary productivity have been invoked as possible drivers of glacial-interglacial climate change and atmospheric CO_2 variability (Brzezinski, 2002; Matsumoto et al., 2002; Sigman & Boyle, 2000; Toggweiler et al., 2006). Our understanding of the role primary productivity plays in the climate system on these timescales is partly attributable to records of opal mass accumulation rates (MAR) in marine sediments (Anderson et al., 2009; Bradtmiller et al., 2009; Charles et al., 1991; Dubois et al., 2010). Many of the records spanning glacial timescales, however, do not have adequate resolution to resolve (sub) millennial-scale changes, which have been shown to influence both the inception and termination of glacial periods (Jouzel et al., 2007). This is partly because the traditional wet-alkaline methods that are used to derive

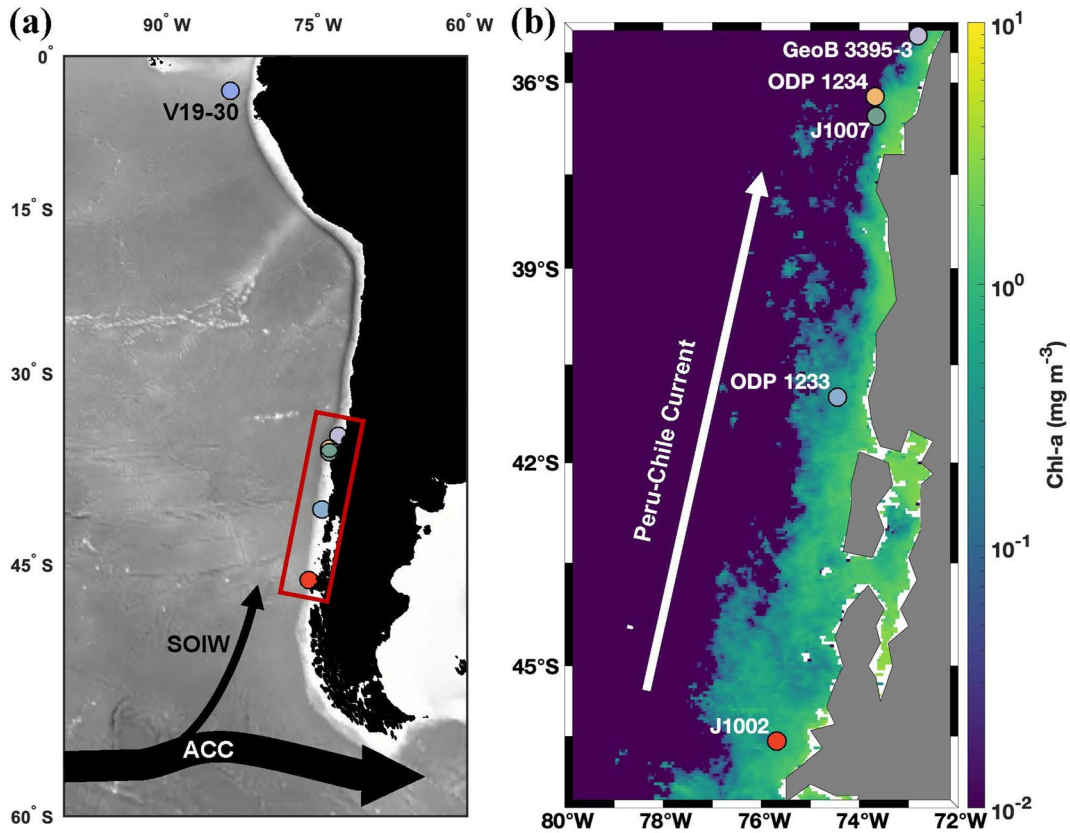

Figure 1. Map of the South Pacific and study region. (a) Core locations of J1002, J1007, and other sites discussed in this paper (Table 1). Black arrows show the path of the Southern Ocean Intermediate Water (SOIW), the surface flow of the Antarctic Circumpolar Current (ACC), and the Peru-Chile Current. (b) Zoomed-in view of the Chilean Margin (red box in panel (a)), with core locations superimposed on mean annual sea-surface chlorophyll-a concentration. J1002 (red), ODP Site 1233 (light blue), J1007 (green), ODP Site 1234 (orange), and GeoB 3395-3 (light purple) are shown. Chlorophyll-a data are from the MODIS-Aqua Level 3 database.

these records are laborious (e.g., Mortlock & Froelich, 1989), which limits the viability of generating continuous, high-resolution records of opal MAR across glacial-interglacial intervals.

One potential avenue to circumvent this obstacle and generate high-resolution opal MAR records is by utilizing the color spectrum of marine sediments derived from core image scanning and spectrometry (Mix et al., 1995; Nederbragt et al., 2000). Generation of sedimentary reflectance spectrometry records upon core recovery is standard for most paleoceanographic coring operations and can provide millimeter-scale resolution of sediment properties (e.g., Mix et al., 1992). These data are often calculated as L* (total light reflected), a* (blue and green), and b* (red and green) values, which have been widely used for core stratigraphy and paleoceanographic reconstructions (e.g., Peterson et al., 2000). For example, Mix et al. (1992) documented a close correlation between high Red/Blue ratios (calculated as b*/a*) and the presence of sulfides in eastern equatorial Pacific (EEP) marine sediment. However, the RGB data extracted from digital section images may be of equal utility since variations in the sediment color often correspond to key oceanic or sediment processes (e.g., primary productivity, terrigenous input, and sediment diagenesis; Nederbragt & Thurow, 2005). Penkrot et al. (2018) reported that the green/blue (G/B) ratio closely tracks biogenic opal in sediment cores taken from the Gulf of Alaska. While these are important observations, the established relationships are qualitative. To leverage these records with potentially millennial- or sub-orbital-scale resolution for reconstructing regional primary productivity, an empirical relationship between RGB variables (e.g., G/B) and a lithologic component (e.g., biogenic opal) must be established.

Recent drilling operations on the south Chilean Margin (D/V *JOIDES Resolution* Exp. 379T funded through the NSF *JR100* program) recovered piston cores to a maximum depth of 100 m to investigate (sub)millennial-scale to glacial-interglacial variability since the penultimate glaciation. Here, we utilize Sites J1002 and J1007 (Figure 1),

which document millennial-to sub-orbital-scale changes in the sediment G/B ratio. The G/B data were initially used onboard as a stratigraphic tool owing to similarities with global climate records (e.g., EDML ice core (the European Project for Ice Coring in Antarctica [EPICA] Dronning Maud Land ice core; EPICA Community Members, 2006). Shipboard lithologic analyses subsequently revealed that sediments enriched with diatoms coincide with high green values, whereas clay-rich sediments corresponded with high blue values (Figure 2). Thus, G/B records in Chilean Margin cores may serve as a paleoceanographic archive of opal percentage in regional sediments.

In this paper, we first explore the conceptual background of the proxy itself, as well as the rationale for using G/B in our stratigraphic efforts. We then test the hypothesis that the G/B record correlates with opal content in sediments on the Chilean Margin by calibrating the proxy to biogenic opal concentrations quantified by traditional methods (Mortlock & Froelich, 1989). Lastly, we use the G/B records and initial core stratigraphy based

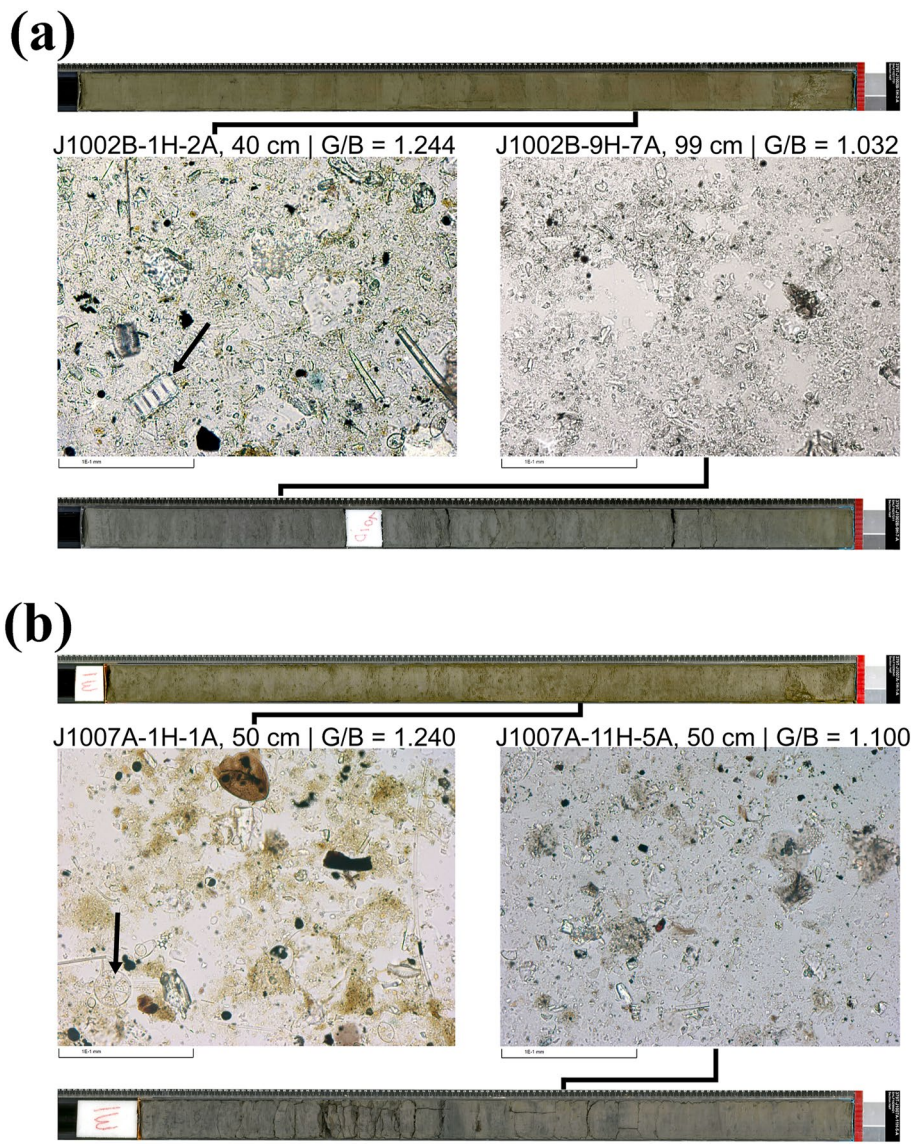

Figure 2. Core photos and smear slide photos representing intervals with high and low G/B values at Site J1002 (a) and Site J1007 (b). Core photos were taken by line-scan camera on Section Half Imaging Logger and smear slide photos under microscope during Expedition 379T. Greener sedimentary intervals (top core sections in both panels) and bluer sedimentary intervals (bottom core sections in both panels) for each site are evident from visual inspection. In both panels (a and b), smear slide photos in the left panels show intervals with abundant diatom presence, corresponding to greener sedimentary intervals, whereas the right panel smear slide images reflect low diatom abundance intervals from bluer intervals. Black arrows show typical diatoms observed in smear slides.

on radiocarbon ages and benthic oxygen isotope records to generate continuous opal MAR records for the last ~150,000 years at Site J1007, offering the highest resolution record of diatom productivity in the south Pacific Ocean through most of the last glacial cycle.

2. Materials and Methods

2.1. Geological and Oceanographic Settings

Our study region in the southeast Pacific Ocean ranges from the central to south Chilean Margin, where the northward deflection of Antarctic Circumpolar Current (ACC) forms the Peru-Chile Current (PCC; a.k.a Humboldt Current) between 40°S and 45°S (Strub, 1998). The northward flowing PCC dominates the surface circulation pattern along the west coast of South America (Figure 1). The poleward flowing Gunther Undercurrent underlies the PCC between 100 and 400 m water depth (Hebbeln et al., 2000; Strub, 1998). Between 500 and 1,200 m water depth flows Antarctic Intermediate Water (AAIW), which forms today at the Subpolar Front by mixing cold, fresh Polar Front waters with Subantarctic Mode Water (Piola & Georgi, 1982; Sallée et al., 2010; Sloyan & Rintoul, 2001). Beneath AAIW sits the northern flowing Antarctic Bottom Water and sluggish Pacific Deep Water (PDW) return flow, which enters the Southern Ocean at mid-depths (Talley, 2013). Coastal upwelling is intensive throughout the year north of 35°S but is restricted to late spring and early fall between 35° and 42°S. South of 42°S, coastal upwelling is inhibited by the prevailing southern westerly winds (Strub, 1998).

The current oceanographic regime makes the Chilean Margin a remarkably productive region in the modern setting. Annual chlorophyll concentration in surface waters along the Chilean Margin reaches up to 4 mg/m^3 (Figure 1b). Annual primary productivity in this region is dominated by diatoms (Abrantes et al., 2007), and based on satellite-measured pigments is estimated to about ~150 gC/m^2/yr off central Chile (31°–37°S) and ~60 gC/m^2/yr along the south Chilean Margin (i.e., south of 37°S; Antoine & Morel, 1996). The latitudinal distribution pattern of opal contents (opal%) and organic carbon contents (C_{org}%) in surface sediment samples reflect the overlying pigment concentration; surface sediment opal% ranges from ~5% off central Chile to ~3% in the south (Romero & Hebbeln, 2003). Despite the high diatom productivity in this region, the opal percentages in the sediments are very low because of the extremely high sedimentation rates on the margin, which can exceed 200 cm/kyr (Hebbeln et al., 2007). High sedimentation rates along the Chilean Margin are largely attributable to significant regional precipitation and high elevations of the Coastal Range and the Andes. Precipitation can vary from <1,000 mm/yr in central Chile to >2,500 mm/yr south of 40°S, leading to increased terrigenous supply in the south (Stuut et al., 2006).

2.2. Study Sites

Sites J1002 and J1007 were recovered from the Chilean Margin using the D/V *JOIDES Resolution* drilling platform during Expedition 379T in Summer 2019 (Figure 1, Table 1). Site J1002 (46° 4.2964′S and 75° 41.2300′W) is located on the south Chilean Margin offshore Northern Patagonia on a bench in the continental slope at a water depth of 1,534 m. At present, this site lies under the northern extent of the ACC and is bathed in PDW. Site J1007 (36° 32.5400′S and 73° 39.9900′W) is located on the continental crust 60 km shoreward of the Chile Trench. With a water depth of 781 m, Site J1007 lies in the heart of modern AAIW (Bova et al., 2021).

Table 1
Site Locations in Figure 1

Core Name	Latitude	Longitude	Water depth (m)	References
J1002	46° 4.30′	75° 41.23′W	1,534	This study
J1007	36° 32.54′	73° 39.99′W	808	This study
ODP Site 1233	41°S	74°27′W	838	Chase et al. (2014)
ODP Site 1234	36°14′S	73°41′W	1,051	Chase et al. (2014)
GeoB 3395-3	35°13′S	72°48.5′W	678	Romero et al. (2006)
V19-30	3°22.98′	83°31.02′W	3,091	Hayes et al. (2011)

Recovered sediments at both sites are assigned to single lithologic units composed primarily of Pleistocene silty clay. Variations of clay contents were presented by natural gamma radiation (NGR) at both sites (Figures S1 and S2 in Supporting Information S1), as higher NGR usually correlated to higher clay contents (Rosenthal et al., 2018). There is a general downhole trend of decreasing NGR at Site J1002 and increasing NGR at Site J1007. Minor biogenic components (primarily diatoms and second foraminifera and nannofossils) and frequent presence of sulfide minerals were found at both sites (Figures S1 and S2 in Supporting Information S1). At J1007, large (2–10 cm) carbonate concretions were found at ~59 and ~97 m, close to the intervals with prominent low magnetic susceptibility. Overall, the dominance of siliciclastic component reflects hemipelagic sedimentation at the two sites (Bova et al., 2021).

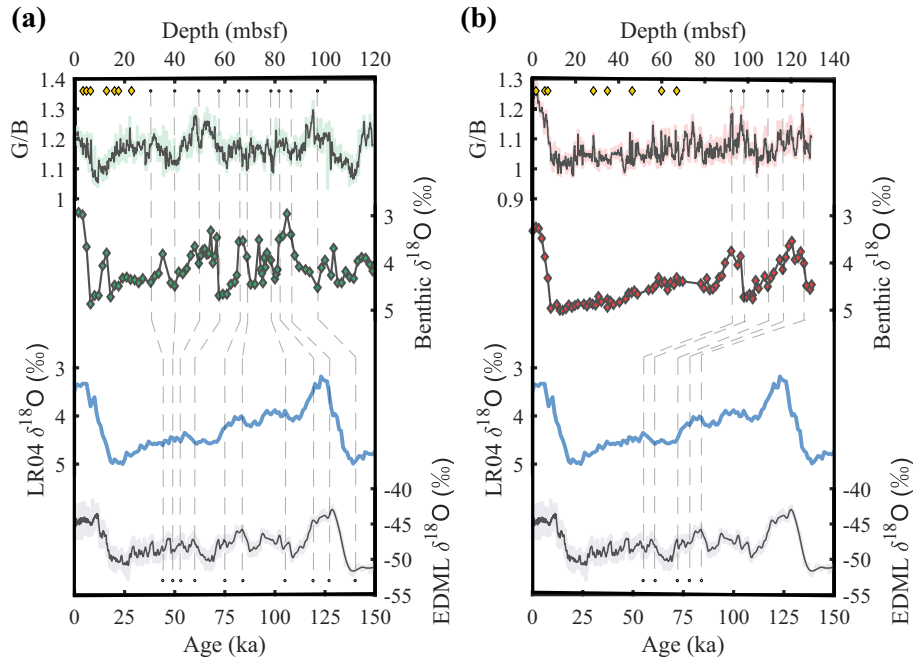

Figure 3. Stratigraphic correlations between Antarctic ice core δ^{18}O (EDML, EPICA Community Members, 2006), LR04 benthic stack (Lisiecki and Raymo, 2005), the G/B, and benthic δ^{18}O for Site J1007 (a) and Site J1002 (b). Age control points from ^{14}C ages are displayed (yellow diamonds). Tie points for visual correlation between benthic δ^{18}O and LR04 are denoted by vertical dashed lines.

2.3. Age Models

Age models for Site J1002 and J1007 (Figures S3 and S4 in Supporting Information S1; see age control points in Table S3 in Supporting Information S1) were based on a combination of AMS radiocarbon dating and the visual correlation of δ^{18}O records of benthic foraminifera to the LR04 benthic stack (Lisiecki and Raymo, 2005). Calendar ages for the upper parts of the core are based on AMS ^{14}C dating of planktonic foraminifera (*Globigerina bulloides*): eight in the upper 67 m of Site J1002 and seven in the upper 23 m at Site J1007, with calendar corrections using IntCal20 (Reimer et al., 2020, Figure 3). Below these depths, stratigraphy is based on visual correlation between benthic foraminifer *Uvigerina* spp. δ^{18}O and the LR04 benthic stack. The *Undatable* program has been used to refine the original age models (Lougheed and Obrochta, 2019), improving the resolution and precision of the opal flux estimate simultaneously (see age-depth figures in Figures S3 and S4 in Supporting Information S1). Comparison with benthic δ^{18}O from the nearby ODP Site 1234 (36°14′S and 73°41′W, 1,015 m; de Bar et al., 2018; Heusser et al., 2006; Robinson et al., 2007) is further applied to constrain the J1007 age model. Nonetheless, we note that the J1007 age model below 66 m is loosely constrained due to limited resolution of the benthic δ^{18}O record. For J1007, the interval between 82 and 86 m is thought to represent the light δ^{18}O "plateau" of Marine Isotope Stage (MIS) 5e. However, the δ^{18}O of this recognized MIS 5e stage are not significantly more depleted than the Holocene as might be expected. Therefore, we caution that it is possible that the real MIS 5e "plateau" was missed due to low sampling resolution and the bottom of J1007 does not reach MIS 5e. This uncertainty has, however, no bearings on the discussion and conclusion of the paper but should be noted by potential users of the core data.

2.4. Sedimentary G/B Ratio

Although extremely high sedimentation rates along the southern Chilean Margin offer the opportunity to generate high-resolution paleoproductivity records, they also pose a few challenges. First, the concentration of biogenic components (e.g., organic carbon% and opal%) are very low (Figures S1 and S2 in Supporting Information S1), approaching the detection limits of the analytical methods. And second, taking advantage of the

high sedimentation rates for generation of high-resolution records using traditional methods is laborious and practically unattainable. For example, to achieve ultra-high resolution in a 100 m sediment core would require collection and analysis of potentially 1,000 of samples. Therefore, scanning methods with 1-cm step can offer valuable information that cannot be obtained from traditional discrete measurements. The advantage of such a method is more in capturing the temporal variability at high resolution than in providing accurate concentrations. The sedimentary G/B ratio is a quantitative method to describe sediment color in the RGB channels of green and blue ranges (Nederbragt & Thurow, 2005). Digital section images were taken on the archive halves of the core using a line-scan camera on the automated Section Half Imaging Logger. Sediment cores were scraped using a glass slide after splitting, and the cleaned flat face of the archive half was immediately imaged to prevent color degradation at a resolution of 10 lines/mm. Data were presented as averaged digitized channels of red, green, and blue, with values ranging from 0 to 255 (Bova et al., 2021). The sedimentary G/B ratio was calculated as the green parameter divided by the blue parameter. It should be noted that the sediment color presented by the RGB channels is different from the L*, a*, b* tristimulus, as the previous one is extracted from digital section images and the latter one is calculated with spectral counts acquired using the light spectrophotometer.

Preliminary results of the shipboard smear slide description suggest a possible link between sediment color and lithology, in agreement with previous work (e.g., Mix et al., 1992, 1995; Nederbragt et al., 2000; Penkrot et al., 2018). Pigments are widely produced by marine algae like diatoms and coccolithophores (Leavitt & Hodgson, 2002). At our study sites, elevated abundance of diatoms is typically found in greener sedimentary intervals (Figure 2). Similar latitudinal distribution patterns of opal%, C_{org}%, and pigment concentrations suggest that diatoms are the dominant group of primary producers along the Chilean Margin (Abrantes et al., 2007; Romero & Hebbeln, 2003; Stuut et al., 2006), thus contributing to most of the pigments in sediments. The primary pigments of diatoms are the green chlorophyll-*a* and the blue-green chlorophyll-*c* (Kuczynska et al., 2015; Stauber & Jeffrey, 1988). Although chlorophyll can be degraded, most of the breakdown products (e.g., chlorins) are still detectable by regular spectrophotometric methods (Reuss et al., 2005). Indeed, downcore pigment records have been used to reconstruct productivity changes in lakes and estuaries for decades (Reuss et al., 2005, 2013). Thus, it has been hypothesized that the color of green is mainly produced by diatom-related pigments in this region. In contrast, cores with a dominance of siliciclastic components and a lower abundance of diatoms are usually found to be bluer (Figure 2). Considering the tremendous terrestrial input commonly found along the Chilean Margin, the siliciclastic component likely produces the blue color. We therefore hypothesize that the sedimentary G/B ratio reflects the relative abundance of biogenic silica in sediments, and based on our calibration, can use it as to quantify diatom productivity along the Chilean Margin over time.

Given the high-temporal variability of the records, the sedimentary G/B ratio has also been a useful tool for stratigraphic correlations among holes drilled during Expedition 379T because it is likely linked to regional climate processes (Bova et al., 2021). Previous studies suggest that Antarctic climate changes have a significant impact on surface water dynamics and terrestrial input off the coast of Chile (Lamy et al., 2004; Kaiser et al., 2007). Regional surface water processes are closely linked to diatom production, hence the green parameter of the sediments. On the other hand, the terrestrial input is assumed to contribute to the blue parameter in sediments. The variation of sedimentary G/B ratio may be sensitive to climate dynamics, making it applicable for stratigraphic correlations. To validate these assumptions, we compare the downcore variations in G/B at J1002 and J1007 with the benthic foraminiferal $\delta^{18}O$ record at each site. The remarkable consistency between the G/B and benthic $\delta^{18}O$ at both sites validates the use of the G/B ratio for stratigraphic correlations along the Chilean Margin (Figure 3). Moreover, G/B ratios at both sites show good correlations with Antarctic ice core $\delta^{18}O$ records, with higher G/B values usually corresponding to warm intervals near Antarctica and lower G/B values corresponding with cold intervals; this observation further demonstrates its utility for stratigraphic correlations (Figure 3). This tool has been especially useful for shipboard correlation as other sedimentary property records in these regions (e.g., magnetic susceptibility, NGR, and other color properties) had muted signals. For example, magnetic susceptibility was widely used for shipboard correlation among holes, but for high sedimentation rate sites—especially those with thick Holocene section that were devoid of any appreciable magnetic susceptibility signal—G/B ratios turned out to be the most applicable stratigraphy tool (Bova et al., 2021).

2.5. Biogenic Opal Analyses

J1002 and J1007 were sampled at intervals spanning the range of G/B values measured at each site to investigate the relationship between opal% and G/B. Biogenic silica concentrations were measured by conventional wet-alkaline digestion, including mineral correction procedures modified after Conley and Schelske (2001). The mineral correction was critical for sediments with relatively low biogenic silica contents as it minimizes the effect of mineral silicates. A total of 22 samples from J1002 and 41 samples from J1007 were analyzed. About 250 mg of freeze-dried sediments were homogenized using a mortar and pestle and digested by 1 mol/L Na_2CO_3 solution in an 80°C water bath. The tubes were shaken quickly for complete digestion every 20 min. Subsamples of 1 mL were taken after 3, 4, and 5 hr of digestion time. Silicate concentration of each subsample was measured by molybdate blue spectrophotometric measurements using an Agilent Cary 60 UV-vis Spectrophotometer at Rutgers University peaked at 812 nm, modified after Mortlock and Froelich (1989) (see detailed experimental and data processing procedure in Text S1 in Supporting Information S1). Ideally, a linear regression was made with the three subsamples, with extrapolation to the intercept providing the final biogenic silica concentration (DeMaster, 1979). Finally, opal% was calculated as biogenic silica concentration multiplied by 2.4 (Mortlock and Froelich, 1989). The standard error of our measurements was 0.35% based on 14 duplicate measurements. Wet-alkaline digestion could be affected by "noise" from clay (Conley & Schelske, 2001). Our mineral correction protocol suggests, however, that clay only contributes to a stable background noise of 0.3% (Figure S5 in Supporting Information S1), which was then removed during the data processing procedure.

2.6. Quantifying U and Th Contents With Shipboard Natural Gamma Radiation Data

Full NGR data for Sites J1002 and J1007 were collected during Expedition 379T. Original NGR spectra obtained on board were composed of numerous peaks for the ^{238}U and ^{232}Th series. Thus, sedimentary contents of thorium (^{232}Th), and uranium (^{238}U) were estimated by identifying and quantifying their characteristic energy peaks using a MATLAB algorithm by De Vleeschouwer et al. (2017). Note that the values reported here are concentration values instead of activity values. De Vleeschouwer et al. (2017) reported the precision of the algorithm as the correlation coefficient between calculated contents and contents measured by mass spectrometry (ICP-MS), which is 0.89 for Th and 0.84 for U based on 245 samples. The accuracy was evaluated by the slope and intercept of the regression line, suggesting a slight overestimation of Th and highly accurate estimates of U content.

3. Results and Discussions

3.1. Calibration of Sedimentary G/B With Measured Opal%

Shipboard sedimentary G/B records exhibit a generally northward increasing trend along the Chilean Margin, in agreement with annual chlorophyll distribution in surface waters (Figure 1b). In addition to lower average values, the G/B for Site J1002 also shows smaller variabilities than J1007. Measured opal% for Site J1002 and Site J1007 vary between 0.36%–4.36% and 1.89%–5.35%, respectively. In general, measured opal% covary with the G/B, with higher measured opal% usually found in greener sediments (Figure 4a). Eight samples from J1007 and one sample from J1002, however, apparently underestimate opal% with respect to G/B (Table S2 in Supporting Information S1). In all cases, these intervals are associated with prominent low values of magnetic susceptibility (Figure 5), which hints to the possibility of diagenetic overprints. This marked decrease of magnetic susceptibility is a widespread phenomenon in sediments of the continental margin, and is usually caused by diagenetic processes within the zone of anaerobic oxidation of methane (Johnson et al., 2021; Riedinger et al., 2005). Distinct diagenetic processes may further induce color alteration of the sediments (Giosan et al., 2002), resulting in mismatch between G/B and measured opal% at these intervals.

At Site J1007, the organic carbon percentage (C_{org}%) correlates well with measured opal% ($n = 21$, $r^2 = 0.51$, $p < 0.05$; Figure 4b), in agreement with the robust correlation between opal% and C_{org}% in the nearby surface sediments (Romero & Hebbeln, 2003). Those samples with potentially underestimated opal%, within low magnetic susceptibility intervals, are similarly offset from the expected values based on average correlation between opal% and C_{org}%. Preliminary shipboard analysis shows the frequent presence of nannofossils and diatoms in sediments along the Chilean Margin (Bova et al., 2021). Discrete measurements onboard suggest that $CaCO_3$% range from 1% to 5% for Site J1007 and 0.3% to 8% for Site J1002 (Figures S1 and S2 in Supporting Information S1). But the

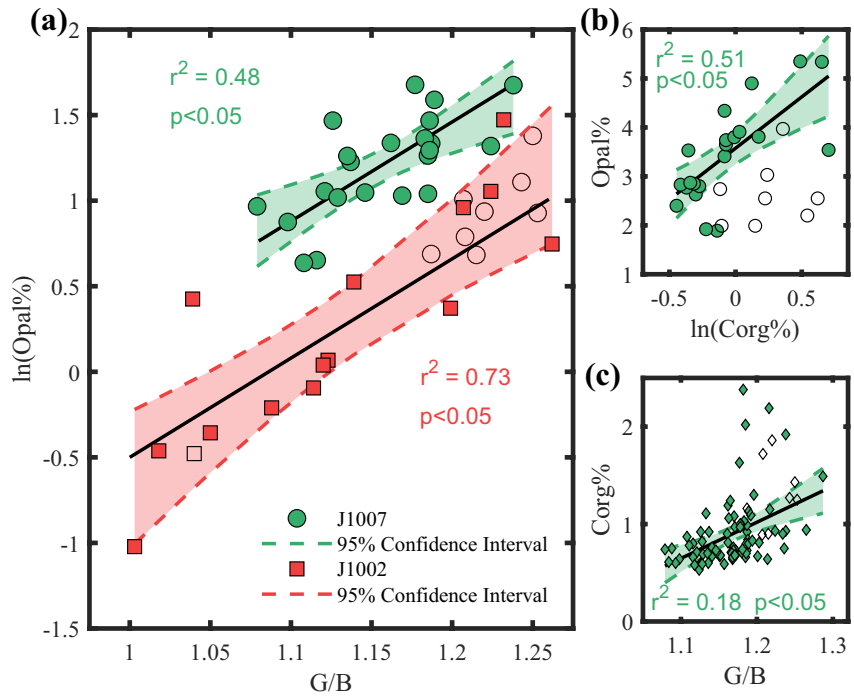

Figure 4. Calibration of the G/B proxy. (a) Correlation between opal% and the sedimentary G/B ratio for Site J1002 (red squares) and Site J1007 (green circles). (b) Correlation between opal% and C_{org}% for Site J1007. (c) Correlation between C_{org}% and sedimentary G/B ratio for Site J1007. Open symbols in all panels represent potentially underestimated opal% data points from low magnetic susceptibility intervals. Shaded areas represent the 95% confidence interval for each regression.

nannofossils only contribute a minor part of the $CaCO_3$ according to estimates from the smear slides (see smear slide photos under cross polar light, Figure S6 in Supporting Information S1). Combining downcore and surface sediment records, it can be deduced that primary productivity in this area is dominated by diatomaceous species, with carbonate nannofossil species as a minor contributor. In contrast, C_{org}% shows only a weak correlation with G/B (Figure 4c), which suggests one or both indicators are impacted by degradation. Nonetheless, most degradation products of chlorophyll retain their original color (Reuss et al., 2005). The color properties of chlorins (a typical chlorophyll degradation product) are measurable by spectrophotometry method in Pleistocene sediments at various sedimentation settings (e.g., Cartagena-Sierra et al., 2021; Gebhardt et al., 2008; Harris et al., 1996; Hodgson et al., 2003), reaching timescales over million years and burial depths of hundreds of meters (Cartagena-Sierra et al., 2021). It is likely the G/B proxy is a more robust indicator and possibly independent of organic matter preservation. Nonetheless, with these caveats in mind, data from low magnetic susceptibly intervals should be considered with higher uncertainty.

Excluding the underestimated data points (20% of entire data set, shown in Figure 5), strong exponential correlations are found between G/B and measured opal% at both sites (J1002: $\ln(y) = 5.8x-6.3$, $n = 14$, $r^2 = 0.73$, $p < 0.05$; J1007: $\ln(y) = 5.8x-5.5$, $n = 22$, $r^2 = 0.48$, $p < 0.05$; where x and y are G/B values and opal%; Figure 4a). The calibrations of J1002 and J1007 show the same slope but different intercept, indicating similar sensitivity of G/B and differences in background colors. Root mean square deviation (RMSD) were calculated based on the differences between measured opal% and the reconstructed opal% derived from G/B values. The RMSD is 0.68% for J1002% and 0.72% for J1007, reflecting the uncertainty of regression models in this study.

Note that while the relationships between G/B, opal%, and C_{org}% are robust, the empirical calibrations are site-specific to J1002 and J1007 and cannot be transferred to other sites, even those in the same region. We hypothesize that variable clay mineralogy along the meridional transect (e.g., Lamy et al., 1998) cause spatial differences in the total "blue" content in the sediments, which were presented by different intercepts of the calibration equations. Although climatically induced changes may substantially influence the mineralogy of the siliciclastic inputs at both J1002 and J1007, such variability is unlikely to cause significant influences on the G/B.

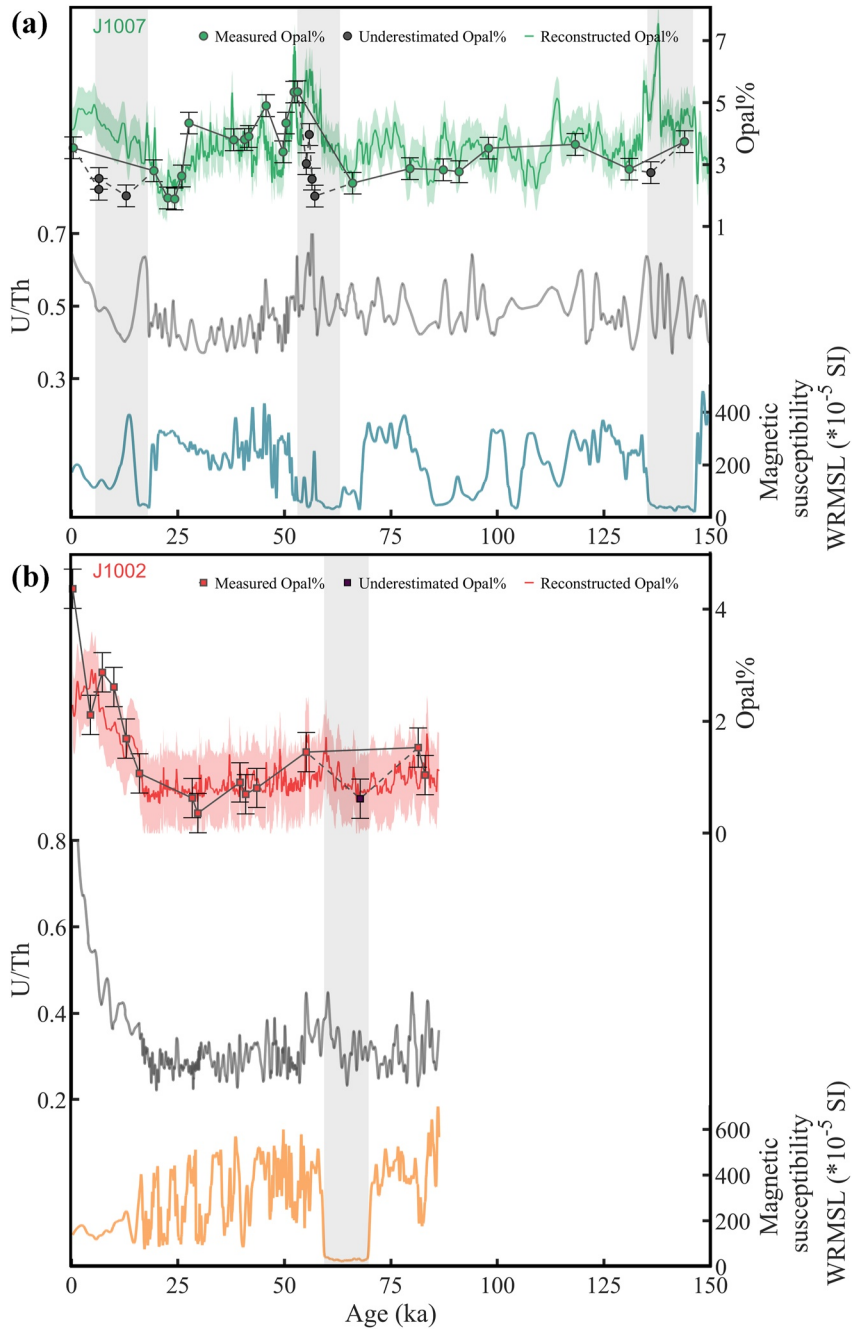

Figure 5. Downcore opal%, U/Th, and magnetic susceptibility records for Site J1007 (a) and Site J1002 (b). Reconstructed opal% for the last ~150 ka at J1007 (green) and 90 ka at J1002 (red) are shown as smoothed solid curves (MATLAB loess smoothing, window = 50) with the ±1 RMSD envelope. Measured opal% (green circles for J1007, red squares for J1002) are superimposed on each reconstructed record. Gray symbols represented potentially underestimated opal% data points from low magnetic susceptibility intervals. The standard error of opal% measurements (0.35%, based on 14 duplicate measurements) was shown as error bar on each data point. Note that we reject those from the calibrations but this does not affect our interpretations of the G/B records. U/Th records are presented as solid gray lines. Magnetic susceptibility at Site J1007 (blue) and Site J1002 (orange) are shown as smoothed solid curves (MATLAB loess smoothing, window = 50). Vertical gray bars denote intervals of low MS coinciding with underestimated opal% data at each site.

For example, chlorite could potentially contribute to the green coloration and is present as an important component of clay mineralogy at the central- and southern Chilean Margin (Lamy et al., 1998). But the chlorite content at ~35°S shows a decreasing trend from the LGM to the Holocene (Lamy et al., 1999), opposing the variation of

G/B record at Site J1007. Similar to X-ray fluorescence (XRF) scanning records of cores, the G/B ratio may also provide a semi-quantitative record that will require a site-specific calibration at each site to convert the relative changes to a record of opal%. It is noteworthy, however, that the two studied sites represent a specific case where the opal concentrations are very low due to dilution from the very high sedimentation rates. It is likely that the method and calibration would be more robust in sites where the contribution of clays and sedimentation rates are lower than those encountered on the Chilean Margin. But the calibrations with low opal% point to the potential utility of G/B proxy in a wide range of depositional settings.

3.2. Reconstructing Opal% Records

Having established the G/B proxy as a tracer of opal% at our study sites, we now use the exponential regression equations above to reconstruct past changes of opal% from the G/B records. Downcore opal% ranges between 0.6%–2.5% and 1.6%–8.8% for J1002 and J1007, respectively (Figure 5). Reconstructed opal% shows relatively large-scale variability at Site J1007, with the highest opal% for the past 150 kyr found during Termination II and MIS 3 (Figure 5a). At Site J1002, reconstructed opal% shows a prominent peak during Holocene, but remains low and stable before Last Glacial Maximum (LGM, 23–19 ka; Figure 5b). At Site J1002, opal% only ranges ∼1% before the LGM, which can be almost entirely attributed to reconstruction uncertainty (2*RMSD = 1.36%, see pink shading in Figure 5). Thus, we caution against the utility of the J1002 opal% reconstruction before the LGM and do not use it for paleoceanographic interpretation.

Over the past 30 kyr, opal% at J1007 and J1002 gradually increases from the last glacial period to the Holocene. During the late Holocene, J1007 opal% is 4%–5%, similar to the opal content of ∼5% in nearby surface sediments (Romero & Hebbeln, 2003). Meanwhile, J1002 opal% of about 2.5% during the Holocene agrees with opal contents of ∼4% in surface sediments at 44°S (Chase et al., 2015; Romero & Hebbeln, 2003). The opal% range for J1007 over the last 30 kyr (2%–6%) is similar to that of two nearby sites, and the variation trend mimics GeoB 3395-3. At Site J1002, the low opal% prior to the last glacial period is attributable to a marked increase in sedimentation rate (>3 m/kyr), which appears to significantly dilute the opal% relative to the Holocene.

Previous opal% reconstructions along the Chilean Margin only covered the past 30 kyr, and vary in a similar range but with different patterns. On the central Chilean Margin, site GeoB 3395-3 (35°13′S and 72°48.5′W, 678 m) has opal% ranging from ∼1.5% to 5% for the past 23 kyr, with the highest values appearing during late Holocene (Romero & Hebbeln, 2003; Romero et al., 2006). The opal% at ODP Site 1234 (36°14′S and 73°41′W, 1,015 m) range from ∼2% to 5% for the last 30 kyr, with peak values occurring during the last glacial period (26–20 ka), but slightly before LGM (Chase et al., 2014). Moreover, it is worth noting that the chlorins content at nearby site GeoB 7165-1 (36°33′S and 73°40′W, 797 m) also increases from the LGM to late Holocene (Mohtadi et al., 2008). Further south, the diatom abundance record from ODP Site 1233 (41°S and 74°27′W, 838 m) is very similar to that of ODP 1234 (Chase et al., 2014). Overall, the consistent range of reconstructed opal% at J1002 and J1007 with nearby sites strongly support the robustness of sedimentary G/B-opal% proxy.

3.3. Sedimentary U/Th

In nature, thorium occurs almost entirely as ^{232}Th while uranium primarily exists as ^{238}U, both of which are primarily supplied to the oceans by riverine runoff (McManus et al., 2006). As a non-redox-sensitive metal, ^{232}Th has low solubility in rivers and oceans, and is largely absorbed on the surface of clay minerals (Harmsen & De Haan, 1980). On the other hand, ^{238}U exist as both soluble U(VI) and insoluble U(IV) phases (Langmuir, 1978). In oxygenated seawater, ^{238}U is present dominantly as a stable U(VI) carbonate complex, with a small fraction associated with particulate organic carbon flux (McManus et al., 2005). Under suboxic conditions, authigenic U accumulates in the sediments as a combination of the bio-authigenic phase associated with settling organic particles and that formed by diffusion of U into sedimentary pore waters (Barnes & Cochran, 1990; Henderson & Anderson, 2003; McManus et al., 2005). Therefore, sedimentary U/Th, which minimizes the influence of variable detrital sources and sedimentation rates (thus the authigenic U burial rate), can be used as a non-quantitative indicator of redox conditions of the sediments.

Both the thorium and uranium contents are higher at Site J1002 than Site J1007, corresponding to larger terrestrial input to the south Chilean Margin. In contrast, U/Th at Site J1007 was found to be higher than that of

J1002 (Figure 5). Higher U/Th reflects more suboxic sedimentary conditions (referring to low dissolved oxygen availability in bottom waters), high organic carbon rain rates, or some combination of both processes (McManus et al., 2006). We observe marked similarities in both trends and magnitudes between measured opal%, G/B-reconstructed opal%, and U/Th profiles at both sites (Figure 5). Authigenic U MARs were also calculated with different assumptions of lithogenic U/Th ratio at J1002 and J1007 (Figure S7 in Supporting Information S1). The authigenic U MAR generally tracks the changes of bulk U/Th at J1007, with increased authigenic U MAR found at the intervals with low magnetic susceptibility. As mentioned before, a marked decrease of magnetic susceptibility is widely linked to diagenetic processes within the zone of anaerobic oxidation of methane (Johnson et al., 2021; Riedinger et al., 2005), likely resulting in elevated U precipitation. At J1002, calculated authigenic U MARs show different patterns to bulk U/Th, suggesting dominant control of sedimentation rate at this site. Taken together, the co-occurrence of high productivity intervals (high opal%, high G/B) and suboxic conditions, as indicated by high U/Th, supports the use of G/B as a proxy of diatom productivity on the Chilean Margin.

3.4. Reconstructed Opal MAR

Previous studies along the Chilean Margin provide only short and relatively low-resolution records of opal MAR (Chase et al., 2014; Hebbeln et al., 2002; Mohtadi & Hebbeln, 2004; Romero et al., 2006). To fill the research gap on sub-orbital-scale variability in diatom productivity, we generated opal MAR records with G/B-derived opal% from Site J1007. Opal MAR at Site J1002 was also calculated for comparisons between J1007 and J1002. Opal MAR was calculated as:

$$\text{Opal MAR} = \text{opal\%} * \rho_{\text{dry}} * \text{LSR} \quad (1)$$

where the opal% is calculated from the calibrated sedimentary G/B ratio, ρ_{dry} is the shipboard-measured dry bulk density of the sediment (g/cm^3), and LSR is the linear sedimentation rate (cm/kyr) as established by J1007 age model. ^{230}Th-normalization was not applied in this study considering that uncertainties inherent in normalization are especially critical for continental margin sediments with shallow water depth and tremendous lithogenic input (Francois et al., 2004).

In general, the sedimentary record of opal MAR shows large-amplitude variation at Site J1007 (Figure 6). Over the last 30 kyr, opal MAR of 2–3 g/cm^2/kyr were found before the LGM, which decreased to ∼1 g/cm^2/kyr during the deglaciation and into the Holocene. The opal flux records from two adjacent sites (GeoB 3395-3 and ODP Site 1234) show a distinct peak of ∼1.5 g/cm^2/kyr during the LGM (Figure 6a; Chase et al., 2014; Romero et al., 2006). Further south, opal MAR from ODP Site 1233 reaches a peak during the last glacial period (1.8 g/cm^2/kyr) and decreases below 0.2 g/cm^2/kyr since 20 ka (Chase et al., 2014). Note that ^{230}Th normalization was applied to opal MAR calculations at ODP Site 1234 and ODP Site 1233, but not at GeoB 3395-3. The opal MAR variation of Site J1007 shows higher levels with longer duration than observed at the other three nearby sites. The difference may be due to the difference in the data sources. The J1007 record is based on continuous high-resolution G/B ratio, whereas the other records are based on low-resolution discrete wet analyses (Figure 5). In fact, comparing the latter with our discrete samples from J1007 suggests a greater consistency among the record in terms of regional changes in opal productivity. We note, however, that changes in sedimentation rate at Site J1007 impart the largest influence on the opal MAR, and the broad peak reflects this. It should be clarified that while the G/B-derived opal% records are in high-resolution, the MAR is in low-resolution due to the limited age model tie points and their respective uncertainties. Thus, the discussion on (sub)millennial-scale opal flux changes is not feasible in this study.

On a longer timescale, the most outstanding features of the Site J1007 opal MAR record are two large peaks, one at ∼50 ka and a secondary peak that we tentatively place at Termination II based on benthic δ^{18}O tuning (Figure 3; Figure 6b). The possibility of an opal flux peak during MIS 3 cannot be ruled out at Site J1002 (Figure 3; Figure S8 in Supporting Information S1). But it would be premature to over interpret the J1002 record given the large uncertainties. Admittedly, effects of lateral sediment transport and sediment focusing could not be ruled out in this study. But significant remobilization that would cause a distinct MAR peak is unlikely, considering the moderate fluctuations of sea level, shore line position, and bottom water condition during MIS 3. Besides that, ^{230}Th-normalized opal fluxes show the same general pattern as opal MAR records at the Chilean Margin for the past 30 ka (Chase et al., 2014). There were inherent tradeoffs with both ^{230}Th-normalized fluxes and the MAR, as the previous one may underestimate the vertical biogenic flux due to potential boundary scavenging,

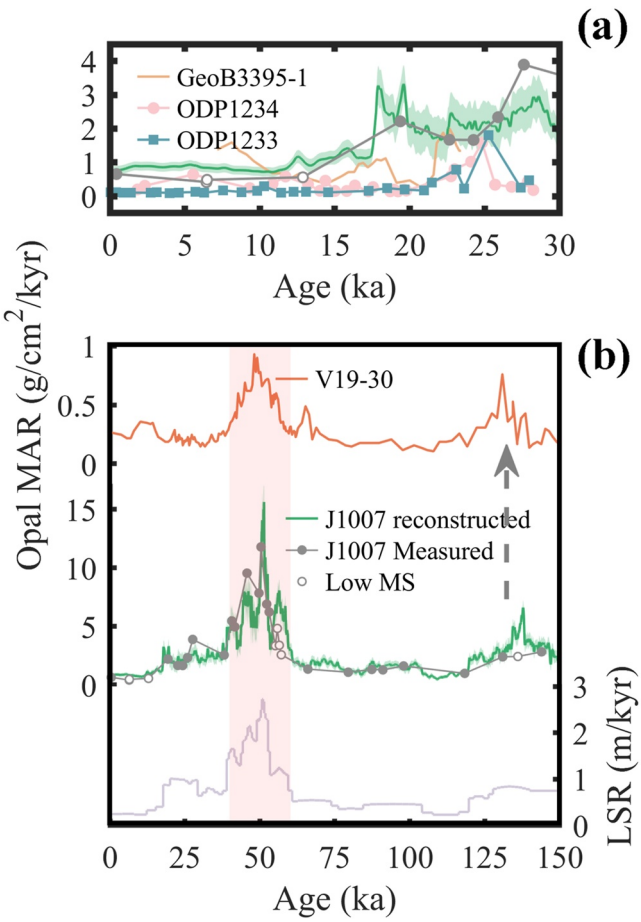

Figure 6. Downcore opal mass accumulation rate (MAR) records from the eastern Pacific Ocean. (a) Opal MAR variation for the last 30 ka at GeoB 3395-3 (yellow; Romero et al., 2006), ODP Site 1234 (pink; Chase et al., 2014), and ODP Site 1233 (blue; Chase et al., 2014). Site J1007 (green) opal MAR are shown as smoothed solid curves (MATLAB loess smoothing, window = 50) with the ±1 uncertainty envelope (by error propagation from 1 RMSD). Gray markers show opal MAR calculated from measured opal% (closed circle) and data points from low magnetic susceptibility (open circle). (b) Opal MAR variation for the last 150 ka at Site J1007 (green) and V19-30 (orange; Hayes et al., 2011). Linear sedimentation rate (LSR) for Site J1007 is shown in the bottom panel. The MIS three peak in opal flux is highlighted with pink shadings. The dashed arrow shows potential correlation between the Site J1007 and EEP opal MAR peak at Termination II based on benthic $\delta^{18}O$ tuning.

while the latter one may overestimate the true vertical flux (Chase et al., 2014). We therefore suggest the 50-ka opal flux peak at Site J1007 results mostly from the vertical biogenic flux. Similar opal flux maxima during MIS 3 have been documented at the site of V19-30 (Figure 6b) and other sites in the EEP (e.g., TR163-31, ME-24; Dubois et al., 2010; Hayes et al., 2011; Kienast et al., 2006). These opal MAR changes along the eastern Pacific basin are further echoed by a Diol index record offshore Southeastern Australia, which infers maximum *Probos-cia* diatom abundance during MIS stages 1, 3, and 5e (Lopes dos Santos et al., 2012).

Previous studies consider enhanced opal preservation as an important contribution to opal MAR in addition to diatom productivity (e.g., Dubois et al., 2010; Tréguer & De La Rocha, 2013). Dissolution is usually found in the intervals with increased dominance of robust species (Shemesh et al., 1989). The smear slide observation shows no significant changes in the diatom assemblage during MIS 3 at Site J1007. On the other hand, enhanced opal preservation related to dust flux (Dubois et al., 2010) have been discussed as possible drivers for the 50-ka flux peak in the EEP, but are unlikely to influence sites at the Chilean Margin. Different from the two clear dust flux peaks during MIS 4 and MIS 2 at the central and the EEP (Winckler et al., 2008), the Fe concentration record from central Chilean margin show higher frequency variability during MIS 2-4 (Kaiser & Lamy, 2010).

Therefore, a common opal flux maxima along the eastern Pacific is more likely referring to a diatom productivity peak rather than an opal preservation peak during MIS 3.

Increased contribution of northern hemisphere waters with higher Si:N has been ruled out as the main control on the EEP opal flux maxima during MIS 3 (Hayes et al., 2011; Kienast et al., 2006), and is less likely a significant source to mid-latitude South Pacific. Therefore, this common 50 ka event along the eastern Pacific meridional transect, paired with a peak diatom productivity offshore Southeastern Australia, implies a climatic connection between the high and low latitudes in the Southern Hemisphere, likely through nutrient-rich intermediate waters exported from the Pacific-sector of the Southern Ocean (Talley, 2013). Southern Ocean Intermediate Waters supply nitrogen, phosphorous, and silicate to the global thermocline, thereby supporting up to 75% of tropical production (Ayers & Strutton, 2013; Sarmiento et al., 2004). The widely presented MIS 3 opal flux peak supports the idea of enhanced Si supply to low latitudes (Hayes et al., 2011), depicting a clear route of "oceanic tunneling" between the Antarctic and the equatorial Pacific (Pena et al., 2008; Spero & Lea, 2002). Moreover, the opal flux at Site J1007 is nearly 10 times greater that of EEP records, implying that mid-latitude continental margins could have served as an important sink for leaking Si from the glacial Southern Ocean (Bradtmiller et al., 2009).

4. Conclusions

Diatom production plays a major role in the biological pump, especially in the Southern Ocean and upwelling regions such as along the EEP and western margins of South American. However, because measuring opal% in sediment is analytically very laborious, obtaining high resolution sedimentary records of opal accumulation is practically impossible, especially in cores with very high-sedimentation rates like those along the Chilean Margin. This study demonstrates that using shipboard measurements of the sedimentary G/B ratio from newly recovered sediment cores on the Chilean Margin, coupled with calibration of discrete samples using traditional methods, can offer a new approach to generate high-resolution paleoceanographic records for reconstructing glacial-interglacial changes in South Pacific diatom productivity. In more detail, we conclude the following:

1. The sedimentary G/B ratio in Chilean Margin sediments can serve as an efficient shipboard stratigraphic tool, where other shipboard data (e.g., magnetic susceptibility) are not conclusive.
2. The G/B records provide high-resolution proxy records for regional changes in diatom productivity over time. The conversion of G/B data to opal% records requires site-specific calibrations from discrete opal% analysis using traditional wet-alkaline digestive methods. Offsets among sites in the G/B ratio to opal% relationships are likely related to lithological effects. Nevertheless, the records suggest that, despite diagenetic effects on biogenic silica and organic matter preservation, the G/B records may more reliably record paleoproductivity, especially in very high sedimentation rates environments where their concentration are diluted.
3. Continuous records of opal MAR on the Chilean Margin over the last ~150,000 years largely tracks existing records from the EEP, with a common opal flux peak at ~50 ka. This suggests a climatic link between high and low latitudes in the South Pacific through intermediate waters.

Appendix A

Ivano W. Aiello[1], Alejandro Avila[2], William Biggs[3], Christopher D. Charles[4], Anson H. Cheung[5], Kimberly deLong[6], Isabel A. Dove[7], Xiaojing Du[5,8], Emily R. Estes[9], Ursula Fuentes[10], Cristina García-Lasanta[11], Steven L. Goldstein[12], Anna Golub[13], Julia Rieke Hagemann[14], Robert G. Hatfield[15], Laura L. Haynes[16], Anya V. Hess[17], Nil Irvali[18], Yael Kiro[19], Minda M. Monteagudo[20], Jonathan E. Lambert[12], William M. Longo[21,22], Sarah McGrath[5], Hailey Riechelson[3], Rebecca S. Robinson[7], John Sarao[23], Adam D. Sproson[24], Shawn Taylor[25], Yusuke Yokoyama[26], and Siyao M. Yu[17]

[1]Moss Landing Marine Laboratories, Moss Landing, CA, USA, [2]Center for Oceanographic Research in the Eastern South Pacific (FONDAP-COPAS), University of Concepción, Concepción, Chile, [3]Department of Marine and Coastal Sciences, Rutgers University, New Brunswick, NJ, USA, [4]Scripps Institution of Oceanography, University of California, San Diego, La Jolla, CA, USA, [5]Department of Earth, Environmental, and Planetary Sciences, Brown University, Providence, RI, USA, [6]Ocean Sciences Department, University of California, Santa Cruz, Santa Cruz, CA, USA, [7]University of Rhode Island Graduate School of Oceanography,

Narragansett, RI, USA, [8]Institute at Brown for Environment and Society, Providence, RI, USA, [9]International Ocean Discovery Program, Texas A&M University, College Station, TX, USA, [10]Hydrographic and Oceanographic Services, Chilean Navy, Valparaíso, Chile, [11]Geology Department, Western Washington University, Bellingham, WA, USA, [12]Lamont-Doherty Earth Observatory, Columbia University, Palisades, NY, USA, [13]Department of Geology and Environmental Geoscience, Lafayette College, Easton, PA, USA, [14]Department of Marine Geology and Paleontology, Alfred Wegener Institute Helmholtz Center for Polar and Marine Research, Bremerhaven, Germany, [15]Department of Geological Sciences, University of Florida, Gainesville, FL, USA, [16]Department of Earth Science and Geography, Vassar College, Poughkeepsie, NY, USA, [17]Department of Earth and Planetary Sciences, Rutgers University, New Brunswick, NJ, USA, [18]Department of Earth Science and Bjerknes Centre for Climate Research, University of Bergen, Bergen, Norway, [19]Department of Earth and Planetary Sciences, Weizmann Institute of Science, Rehovot, Israel, [20]School of Earth and Atmospheric Sciences, Georgia Institute of Technology, Atlanta, GA, USA, [21]Department of Environmental Studies, Macalester College, Saint Paul, MN, USA, [22]Division of Environmental Health Sciences, University of Minnesota, Minneapolis, MN, USA, [23]College of Geosciences, Texas A&M University, College Station, TX, USA, [24]Biogeochemistry Research Center, JAMSTEC, Yokosuka, Japan, [25]Department of Geological Sciences and Environmental Studies, Binghamton University, Binghamton, NY, USA, [26]Atmosphere and Ocean Research Institute, The University of Tokyo, Chiba, Japan

Data Availability Statement

All data used for this study are available at: https://www.ncei.noaa.gov/access/paleo-search/study/36494.

Acknowledgments
The authors would like to thank the captain and crew of the D/V *JOIDES Resolution* and JRSO for their tireless efforts during the inaugural JR100 expedition. C. Li, V. J. Clementi, and Y. Rosenthal designed the experiment. C. Li and V. J. Clementi carried out shore-based geochemical analyses, prepared figures, and wrote the manuscript. S. C. Bova, Y. Rosenthal, and L. B. Childress organized and managed the expedition. J. D. Wright co-led shipboard stratigraphic efforts with G/B. Expedition 379T Scientists assisted in the collection of G/B data and interpretation of shipboard sedimentological data. All authors contributed to the interpretation of shipboard data. The expedition was funded by the NSF grant OCE-1756241. C. Li was supported by the Ministry of Science and Technology of China (Grant 2018YFE0202401). This study was funded by the NSF grant OCE-1756241 to S. C. Bova and Y. Rosenthal, V. J. Clementi was supported by the NETL Methane Hydrates Fellowship Program. The authors thank Ivano Aiello for the valuable comments on method and lithology section. The authors also thank Steve Phillips and an anonymous reviewer for their useful and critical reviews that help us improve this paper.

References

Abrantes, F., Lopes, C., Mix, A., & Pisias, N. (2007). Diatoms in Southeast Pacific surface sediments reflect environmental properties. *Quaternary Science Reviews*, *26*(1–2), 155–169. https://doi.org/10.1016/j.quascirev.2006.02.022

Anderson, R. F., Ali, S., Bradtmiller, L. I., Nielsen, S. H., Fleisher, M. Q., Anderson, B. E., & Burckle, L. H. (2009). Wind-driven upwelling in the Southern Ocean and the deglacial rise in atmospheric CO_2. *Science*, *323*(5920), 1443–1448. https://doi.org/10.1126/science.1167441

Antoine, D., & Morel, A. (1996). Oceanic primary production: 1. Adaptation of a spectral light-photosynthesis model in view of application to satellite chlorophyll observations. *Global Biogeochemical Cycles*, *10*(1), 43–55. https://doi.org/10.1029/95GB02831

Ayers, J. M., & Strutton, P. G. (2013). Nutrient variability in subantarctic mode waters forced by the southern annular mode and ENSO. *Geophysical Research Letters*, *40*(13), 3419–3423. https://doi.org/10.1002/grl.50638

Barnes, C., & Cochran, J. (1990). Uranium removal in oceanic sediments and the oceanic U balance. *Earth and Planetary Science Letters*, *97*(1–2), 94–101. https://doi.org/10.1016/0012-821x(90)90101-3

Bova, S. C., Rosenthal, Y., Childress, L. B., & Expedition 379T Scientists. (2021). Digging deeper with the JR100: Extending high resolution paleoclimate records from the Chilean Margin to the Eemian. Personal communication. Retrieved from https://zenodo.org/record/5553428#.YV4q6y2cbIE

Bradtmiller, L. I., Anderson, R. F., Fleisher, M. Q., & Burckle, L. H. (2009). Comparing glacial and Holocene opal fluxes in the Pacific sector of the Southern Ocean. *Paleoceanography*, *24*(2). https://doi.org/10.1029/2008pa001693

Brzezinski, M. A. (2002). A switch from $Si(OH)_4$ to NO^{3-} depletion in the glacial Southern Ocean. *Geophysical Research Letters*, *29*(12), 1564. https://doi.org/10.1029/2001gl014349

Cartagena-Sierra, A., Berke, M. A., Robinson, R. S., Marcks, B., Castañeda, I. S., Starr, A., et al. (2021). Latitudinal migrations of the subtropical front at the Agulhas Plateau through the mid-Pleistocene transition. *Paleoceanography and Paleoclimatology*, *36*(7). https://doi.org/10.1029/2020pa004084

Charles, C. D., Froelich, P. N., Zibello, M. A., Mortlock, R. A., & Morley, J. J. (1991). Biogenic opal in Southern Ocean sediments over the last 450,000 years: Implications for surface water chemistry and circulation. *Paleoceanography*, *6*(6), 697–728. https://doi.org/10.1029/91PA02477

Chase, Z., Kohfeld, K. E., & Matsumoto, K. (2015). Controls on biogenic silica burial in the Southern Ocean. *Global Biogeochemical Cycles*, *29*(10), 1599–1616. https://doi.org/10.1002/2015gb005186

Chase, Z., McManus, J., Mix, A. C., & Muratli, J. (2014). Southern-ocean and glaciogenic nutrients control diatom export production on the Chile Margin. *Quaternary Science Reviews*, *99*, 135–145. https://doi.org/10.1016/j.quascirev.2014.06.015

Conley, D. J., & Schelske, C. L. (2001). Biogenic silica. In J. P. Smol, H. J. B. Birks, W. M. Last, R. S. Bradley, & K. Alverson (Eds.), *Tracking environmental change using lake sediments: Terrestrial, algal, and siliceous indicators* (pp. 281–293). Springer Netherlands.

de Bar, M. W., Stolwijk, D. J., McManus, J. F., Sinninghe Damsté, J. S., & Schouten, S. (2018). A Late Quaternary climate record based on long-chain diol proxies from the Chilean Margin. *Climate of the Past*, *14*(11), 1783–1803. https://doi.org/10.5194/cp-14-1783-2018

DeMaster, D. J. (1979). *The marine budgets of silica and Ph.D. dissertation* (p. 308). Yale University.

De Vleeschouwer, D., Dunlea, A. G., Auer, G., Anderson, C. H., Brumsack, H., de Loach, A., et al. (2017). Quantifying K, U, and Th contents of marine sediments using shipboard natural gamma radiation spectra measured on DV *JOIDES Resolution*. *Geochemistry, Geophysics, Geosystems*, *18*(3), 1053–1064. https://doi.org/10.1002/2016gc006715

Dubois, N., Kienast, M., Kienast, S., Calvert, S. E., François, R., & Anderson, R. F. (2010). Sedimentary opal records in the eastern equatorial Pacific: It is not all about leakage. *Global Biogeochemical Cycles*, *24*(4). https://doi.org/10.1029/2010gb003821

EPICA Community Members. (2006). One-to-one coupling of glacial climate variability in Greenland and Antarctica. *Nature*, *444*(7116), 195–198. https://doi.org/10.1038/nature05301

Francois, R., Frank, M., Rutgers van der Loeff, M. M., & Bacon, M. P. (2004). ^{230}Th normalization: An essential tool for interpreting sedimentary fluxes during the late Quaternary. *Paleoceanography*, *19*(1). https://doi.org/10.1029/2003pa000939

Gebhardt, H., Sarnthein, M., Grootes, P. M., Kiefer, T., Kuehn, H., Schmieder, F., & Röhl, U. (2008). Paleonutrient and productivity records from the subarctic North Pacific for Pleistocene glacial terminations I to V. *Paleoceanography*, *23*(4). https://doi.org/10.1029/2007pa001513

Giosan, L., Flood, R. D., & Aller, R. C. (2002). Paleoceanographic significance of sediment color on western North Atlantic drifts: I. Origin of color. *Marine Geology*, *189*(1–2), 25–41. https://doi.org/10.1016/s0025-3227(02)00321-3

Harmsen, K., & De Haan, F. A. M. (1980). Occurrence and behaviour of uranium and thorium in soil and water. *Netherlands Journal of Agricultural Science*, *28*(1), 40–62. https://doi.org/10.18174/njas.v28i1.17043

Harris, P. G., Zhao, M., Rosell-Melé, A., Tiedemann, R., Sarnthein, M., & Maxwell, J. R. (1996). Chlorin accumulation rate as a proxy for quaternary marine primary productivity. *Nature*, *383*(6595), 63–65. https://doi.org/10.1016/S0025-3227(02)00321-3

Hayes, C. T., Anderson, R. F., & Fleisher, M. Q. (2011). Opal accumulation rates in the equatorial Pacific and mechanisms of deglaciation. *Paleoceanography*, *26*(1), PA1207. https://doi.org/10.1029/2010pa002008

Hebbeln, D., Lamy, F., Mohtadi, M., & Echtler, H. (2007). Tracing the impact of glacial-interglacial climate variability on erosion of the southern Andes. *Geology*, *35*(2), 131. https://doi.org/10.1130/g23243a.1

Hebbeln, D., Marchant, M., Freudenthal, T., & Wefer, G. (2000). Surface sediment distribution along the Chilean continental slope related to upwelling and productivity. *Marine Geology*, *164*(3–4), 119–137. https://doi.org/10.1016/s0025-3227(99)00129-2

Hebbeln, D., Marchant, M., & Wefer, G. (2002). Paleoproductivity in the southern Peru-Chile Current through the last 33 000 yr. *Marine Geology*, *186*(3–4), 487–504. https://doi.org/10.1016/S0025-3227(02)00331-6

Henderson, G. M., & Anderson, R. F. (2003). The U-series toolbox for paleoceanography. *Reviews in Mineralogy and Geochemistry*, *52*(1), 493–531. https://doi.org/10.1515/9781501509308-017

Heusser, L., Heusser, C., Mix, A., & McManus, J. (2006). Chilean and Southeast Pacific paleoclimate variations during the last glacial cycle: Directly correlated pollen and $\delta^{18}O$ records from ODP site 1234. *Quaternary Science Reviews*, *25*(23–24), 3404–3415. https://doi.org/10.1016/j.quascirev.2006.03.011

Hodgson, D. A., McMinn, A., Kirkup, H., Cremer, H., Gore, D., Melles, M., et al. (2003). Colonization, succession, and extinction of marine floras during a glacial cycle: A case study from the Windmill Islands (east Antarctica) using biomarkers. *Paleoceanography*, *18*(3). https://doi.org/10.1029/2002pa000775

Johnson, J. E., Phillips, S. C., Clyde, W. C., Giosan, L., & Torres, M. E. (2021). Isolating detrital and diagenetic signals in magnetic susceptibility records from methane-bearing marine sediments. *Geochemistry, Geophysics, Geosystems*, *22*(9), e2021GC009867. https://doi.org/10.1029/2021GC009867

Jouzel, J., Masson-Delmotte, V., Cattani, O., Dreyfus, G., Falourd, S., Hoffmann, G., et al. (2007). Orbital and millennial Antarctic climate variability over the past 800,000 years. *Science*, *317*(5839), 793–796. https://doi.org/10.1126/science.1141038

Kaiser, J., & Lamy, F. (2010). Links between Patagonian Ice Sheet fluctuations and Antarctic dust variability during the last glacial period (MIS 4-2). *Quaternary Science Reviews*, *29*(11–12), 1464–1471. https://doi.org/10.1016/j.quascirev.2010.03.005

Kaiser, J., Lamy, F., Arz, H. W., & Hebbeln, D. (2007). Dynamics of the millennial-scale sea surface temperature and Patagonian Ice Sheet fluctuations in southern Chile during the last 70 kyr (ODP Site 1233). *Quaternary International*, *161*(1), 77–89. https://doi.org/10.1016/j.quaint.2006.10.024

Kienast, S. S., Kienast, M., Jaccard, S., Calvert, S. E., & François, R. (2006). Testing the silica leakage hypothesis with sedimentary opal records from the eastern equatorial Pacific over the last 150 kyrs. *Geophysical Research Letters*, *33*(15), L15607. https://doi.org/10.1029/2006GL026651

Kuczynska, P., Jemiola-Rzeminska, M., & Strzalka, K. (2015). Photosynthetic pigments in diatoms. *Marine Drugs*, *13*(9), 5847–5881. https://doi.org/10.3390/md13095847

Lamy, F., Hebbeln, D., & Wefer, G. (1998). Terrigenous sediment supply along the Chilean continental margin: Modern regional patterns of texture and composition. *Geologische Rundschau*, *87*(3), 477–494. https://doi.org/10.1007/s005310050223

Lamy, F., Hebbeln, D., & Wefer, G. (1999). High-resolution marine record of climatic change in mid-latitude Chile during the last 28,000 years based on terrigenous sediment parameters. *Quaternary Research*, *51*(1), 83–93. https://doi.org/10.1006/qres.1998.2010

Lamy, F., Kaiser, J., Ninnemann, U., Hebbeln, D., Arz, H. W., & Stoner, J. (2004). Antarctic timing of surface water changes off Chile and Patagonian ice sheet response. *Science*, *304*(5679), 1959–1962. https://doi.org/10.1126/science.1097863

Langmuir, D. (1978). Uranium solution-mineral equilibria at low temperatures with applications to sedimentary ore deposits. *Geochimica et Cosmochimica Acta*, *42*(6), 547–569. https://doi.org/10.1016/0016-7037(78)90001-7

Leavitt, P. R., & Hodgson, D. A. (2002). Sedimentary pigments. In *Tracking environmental change using lake sediments* (pp. 295–325).

Lisiecki, L. E., & Raymo, M. E. (2005). A Pliocene-Pleistocene stack of 57 globally distributed benthic $\delta^{18}O$ records. *Paleoceanography*, *20*(1). https://doi.org/10.1029/2004pa001071

Lopes dos Santos, R. A., Wilkins, D., De Deckker, P., & Schouten, S. (2012). Late quaternary productivity changes from offshore southeastern Australia: A biomarker approach. *Palaeogeography, Palaeoclimatology, Palaeoecology*, *363–364*, 48–56. https://doi.org/10.1016/j.palaeo.2012.08.013

Lougheed, B. C., & Obrochta, S. P. (2019). A rapid, deterministic age-depth modeling routine for geological sequences with inherent depth uncertainty. *Paleoceanography and Paleoclimatology*, *34*(1), 122–133. https://doi.org/10.1029/2018pa003457

Matsumoto, K., Sarmiento, J. L., & Brzezinski, M. A. (2002). Silicic acid leakage from the Southern Ocean: A possible explanation for glacial atmospheric pCO_2. *Global Biogeochemical Cycles*, *16*(3), 5-1–5-23. https://doi.org/10.1029/2001gb001442

McManus, J., Berelson, W. M., Klinkhammer, G. P., Hammond, D. E., & Holm, C. (2005). Authigenic uranium: Relationship to oxygen penetration depth and organic carbon rain. *Geochimica et Cosmochimica Acta*, *69*(1), 95–108. https://doi.org/10.1016/j.gca.2004.06.023

McManus, J., Berelson, W. M., Severmann, S., Poulson, R. L., Hammond, D. E., Klinkhammer, G. P., & Holm, C. (2006). Molybdenum and uranium geochemistry in continental margin sediments: Paleoproxy potential. *Geochimica et Cosmochimica Acta*, *70*(18), 4643–4662. https://doi.org/10.1016/j.gca.2006.06.1564

Mix, A. C., Harris, S. E., & Janecek, T. R. (1995). Estimating lithology from nonintrusive reflectance spectra: Leg 138. *Proceedings of the Ocean Drilling Program. Scientific Results*, *138*. https://doi.org/10.2973/odp.proc.sr.138.121.1995

Mix, A. C., Rugh, W., Pisias, N. G., & Veirs, S. (1992). Color reflectance spectroscopy: A tool for rapid characterization of deep-sea sediments. In *Paper presented at the Proceedings of the Ocean Drilling Program, Part A, Initial Report*.

Mohtadi, M., & Hebbeln, D. (2004). Mechanisms and variations of the paleoproductivity off northern Chile (24°S-33°S) during the last 40,000 years. *Paleoceanography*, *19*(2). https://doi.org/10.1029/2004pa001003

Mohtadi, M., Rossel, P., Lange, C. B., Pantoja, S., Böning, P., Repeta, D. J., & Brumsack, H.-J. (2008). Deglacial pattern of circulation and marine productivity in the upwelling region off central-south Chile. *Earth and Planetary Science Letters*, *272*(1–2), 221–230. https://doi.org/10.1016/j.epsl.2008.04.043

Mortlock, R. A., & Froelich, P. N. (1989). A simple method for the rapid determination of biogenic opal in pelagic marine sediments. *Deep Sea Research Part A. Oceanographic Research Papers*, *36*(9), 1415–1426. https://doi.org/10.1016/0198-0149(89)90092-7

Nederbragt, A. J., & Thurow, J. W. (2005). Digital sediment colour analysis as a method to obtain high resolution climate proxy records. In *Image analysis, sediments and paleoenvironments* (pp. 105–124). Springer.
Nederbragt, A. J., Thurow, J. W., & Merrill, R. B. (2000). Color records from the California margin: Proxy indicators for sediment composition and climatic change. *Proceedings of the Ocean Drilling Program. Scientific Results*, *167*, 319–329.
Pena, L. D., Cacho, I., Ferretti, P., & Hall, M. A. (2008). El Niño–Southern Oscillation–like variability during glacial terminations and interlatitudinal teleconnections. *Paleoceanography*, *23*(3). https://doi.org/10.1029/2008PA001620
Penkrot, M. L., Jaeger, J. M., Cowan, E. A., St-Onge, G., & LeVay, L. (2018). Multivariate modeling of glacimarine lithostratigraphy combining scanning XRF, multisensory core properties, and CT imagery: IODP site U1419. *Geosphere*, *14*(4), 1935–1960. https://doi.org/10.1130/ges01635.1
Peterson, L. C., Haug, G. H., Hughen, K. A., & Röhl, U. (2000). Rapid changes in the hydrologic cycle of the tropical Atlantic during the last glacial. *Science*, *290*(5498), 1947–1951. https://doi.org/10.1126/science.290.5498.1947
Piola, A. R., & Georgi, D. T. (1982). Circumpolar properties of Antarctic intermediate water and Subantarctic Mode water. Deep sea research Part A. *Oceanographic Research Papers*, *29*(6), 687–711. https://doi.org/10.1016/0198-0149(82)90002-4
Reimer, P. J., Austin, W. E. N., Bard, E., Bayliss, A., Blackwell, P. G., Bronk Ramsey, C., & Talamo, S. (2020). The IntCal20 Northern hemisphere radiocarbon age calibration curve (0–55 cal kBP). *Radiocarbon*, *62*(4), 725–757. https://doi.org/10.1017/rdc.2020.41
Reuss, N., Conley, D. J., & Bianchi, T. S. (2005). Preservation conditions and the use of sediment pigments as a tool for recent ecological reconstruction in four Northern European estuaries. *Marine Chemistry*, *95*(3), 283–302. https://doi.org/10.1016/j.marchem.2004.10.002
Reuss, N. S., Anderson, N. J., Fritz, S. C., & Simpson, G. L. (2013). Responses of microbial phototrophs to late-Holocene environmental forcing of lakes in south-west Greenland. *Freshwater Biology*, *58*(4), 690–704. https://doi.org/10.1111/fwb.12073
Riedinger, N., Pfeifer, K., Kasten, S., Garming, J. F. L., Vogt, C., & Hensen, C. (2005). Diagenetic alteration of magnetic signals by anaerobic oxidation of methane related to a change in sedimentation rate. *Geochimica et Cosmochimica Acta*, *69*(16), 4117–4126. https://doi.org/10.1016/j.gca.2005.02.004
Robinson, R. S., Mix, A., & Martinez, P. (2007). Southern Ocean control on the extent of denitrification in the southeast Pacific over the last 70 ka. *Quaternary Science Reviews*, *26*(1–2), 201–212. https://doi.org/10.1016/j.quascirev.2006.08.005
Romero, O., & Hebbeln, D. (2003). Biogenic silica and diatom thanatocoenosis in surface sediments below the Peru–Chile current: Controlling mechanisms and relationship with productivity of surface waters. *Marine Micropaleontology*, *48*(1), 71–90. https://doi.org/10.1016/S0377-8398(02)00161-5
Romero, O. E., Kim, J.-H., & Hebbeln, D. (2006). Paleoproductivity evolution off central Chile from the Last Glacial Maximum to the Early Holocene. *Quaternary Research*, *65*(3), 519–525. https://doi.org/10.1016/j.yqres.2005.07.003
Rosenthal, Y., Holbourn, A. E., Kulhanek, D. K., Aiello, I. W., Babila, T. L., Bayon, G., et al. (2018). Expedition 363 summary. In *Proceedings of the International Ocean Discovery Program*.
Sallée, J.-B., Speer, K., Rintoul, S., & Wijffels, S. (2010). Southern Ocean thermocline ventilation. *Journal of Physical Oceanography*, *40*(3), 509–529. https://doi.org/10.1175/2009JPO4291.1
Sarmiento, J. L., Gruber, N., Brzezinski, M., & Dunne, J. (2004). High-latitude controls of thermocline nutrients and low latitude biological productivity. *Nature*, *427*(6969), 56–60. https://doi.org/10.1038/nature02127
Shemesh, A., Burckle, L. H., & Froelich, P. N. (1989). Dissolution and preservation of Antarctic diatoms and the effect on sediment thanatocoenoses. *Quaternary Research*, *31*(2), 288–308. https://doi.org/10.1016/0033-5894(89)90010-0
Sigman, D. M., & Boyle, E. A. (2000). Glacial/interglacial variations in atmospheric carbon dioxide. *Nature*, *407*(6806), 859–869. https://doi.org/10.1038/35038000
Sloyan, B. M., & Rintoul, S. R. (2001). The Southern Ocean limb of the global deep overturning circulation. *Journal of Physical Oceanography*, *31*(1), 143–173. https://doi.org/10.1175/1520-0485(2001)031<0143:Tsolot>2.0.Co;2
Spero, H. J., & Lea, D. W. (2002). The cause of carbon isotope minimum events on glacial terminations. *Science*, *296*(5567), 522–525. https://doi.org/10.1126/science.1069401
Stauber, J. L., & Jeffrey, S. W. (1988). Photosynthetic pigments in fifty-one species of marine diatoms. *Journal of Phycology*, *24*(2), 158–172. https://doi.org/10.1111/j.1529-8817.1988.tb04230.x
Strub, P. T. (1998). Coastal ocean circulation off Western South America. *The Global Coastal Ocean. Regional Studies and Syntheses*, 273–315. Retrieved from https://ci.nii.ac.jp/naid/20001225871/en/
Stuut, J. B. W., Marchant, M., Kaiser, J., Lamy, F., Mohtadi, M., Romero, O., & Hebbeln, D. (2006). The late quaternary paleoenvironment of Chile as seen from marine archives. *Geographica Helvetica*, *61*(2), 135–151. https://doi.org/10.5194/gh-61-135-2006
Talley, L. (2013). Closure of the global overturning circulation through the Indian, Pacific, and Southern Oceans: Schematics and transports. *Oceanography*, *26*(1), 80–97. https://doi.org/10.5670/oceanog.2013.07
Toggweiler, J. R., Russell, J. L., & Carson, S. R. (2006). Midlatitude westerlies, atmospheric CO_2, and climate change during the ice ages. *Paleoceanography*, *21*(2). https://doi.org/10.1029/2005pa001154
Tréguer, P. J., & De La Rocha, C. L. (2013). The world ocean silica cycle. *Annual Review of Marine Science*, *5*(1), 477–501. https://doi.org/10.1146/annurev-marine-121211-172346
Winckler, G., Anderson, R. F., Fleisher, M. Q., McGee, D., & Mahowald, N. (2008). Covariant glacial-interglacial dust fluxes in the equatorial Pacific and Antarctica. *Science*, *320*(5872), 93–96. https://doi.org/10.1126/science.1150595

References From the Supporting Information

Conley, D. J., & Schelske, C. L. (2001). Biogenic silica. In J. P. Smol, H. J. B. Birks, W. M. Last, R. S. Bradley, & K. Alverson (Eds.), *Tracking environmental change using lake sediments: Terrestrial, algal, and siliceous indicators* (pp. 281–293). Springer Netherlands.
DeMaster, D. J. (1979). *The marine budgets of silica and Ph.D. dissertation* (p. 308). Yale University.
Lisiecki, L. E., & Raymo, M. E. (2005). A Pliocene-Pleistocene stack of 57 globally distributed benthic $\delta^{18}O$ records. *Paleoceanography*, *20*(1). https://doi.org/10.1029/2004pa001071
Lougheed, B. C., & Obrochta, S. P. (2019). A rapid, deterministic age-depth modeling routine for geological sequences with inherent depth uncertainty. *Paleoceanography and Paleoclimatology*, *34*(1), 122–133. https://doi.org/10.1029/2018pa003457
Mortlock, R. A., & Froelich, P. N. (1989). A simple method for the rapid determination of biogenic opal in pelagic marine sediments. *Deep Sea Research Part A. Oceanographic Research Papers*, *36*(9), 1415–1426. https://doi.org/10.1016/0198-0149(89)90092-7